Journal of Scientific & Industrial Research
Vol. 80, October 2021, pp. 875-886

HoEnTOA: Holoentropy and Taylor Assisted Optimization based Novel Image Quality Enhancement Algorithm for Multi-Focus Image Fusion

Vineeta Singh* and Vandana Dixit Kaushik

Department of Computer Science and Engineering, Harcourt Butler Technical University
East Campus, Nawabganj, Kanpur, Uttar Pradesh 208 002, India

Received 08 July 2021; revised 14 September 2021; accepted 15 September 2021

In machine vision as well as image processing applications, multi-focus image fusion strategy carries a prominent exposure. Normally, image fusion is a method of merging of information extracted out of two or more than two source images fused to produce a solitary image, which is much more instructive as well as much suitable for computer processing and visual perception. In this research paper authors have devised a novel image quality enhancement algorithm by fusing multi-focus images, in short, termed as HoEnTOA. Initially, contourlet transform is incorporated to both of the input images for generation of four respective sub-bands of each of input image. After converting into sub-bands further holoentropy along with proposed HoEnTOA is introduced to fuse multi-focus images. Here, the developed HoEnTOA is integration of Taylor series with ASSCA. After fusion, the inverse contourlet transform is incorporated for obtaining last fused image. Thus, the proposed HoEnTOA effectively performs the image fusion and has demonstrated better performance utilizing the five metrics i.e. Root Mean Square Error with a minimum value of 3.687, highest universal quality index value of 0.984, maximum Peak Signal to Noise Ratio of 42.08dB, maximal structural similarity index measurement of 0.943, as well as maximum mutual information of 1.651.

Keywords: Contourlet transform, Medical imaging, Optimization based fusion technique, Taylor series, Two level image fusion

Introduction

Normally, multi image fusion intends to combine two or more than two images, which is captured by various camera locations of similar picture to produce other better image with sharp content and identical focus. It is generally not possible to get an image with each of the related object in focus because of imperfect depth-of-focus in optical lenses.[1,2] Optics of lenses with high degree of intensification experiences due to restricted depth of field issues. The depth of field becomes lesser because of, high intensification and focal length of lens. Thus, lesser objects in an image are focused although[3,4], at certain time people desire to gain an image with more focused/visual clarity objects. The perfect circumstance in total image is that it is focus or in apparent, which directs to emergence of multi-focus image fusion technology. The concept of multi-focus image fusion involves various images with dissimilar focus location to be combined for generating new fused image with unlimited depth of field. The main intention is to improve perceptible depth of filed by combination of objects in various fields of focus. Therefore, image fusion technology plays a significant job for many application domains, like biomedical imaging as well as computer vision. Moreover, multi focus image fusion is a broader as well as inevitable area of research in image processing field.[5,6] Typically, several images of similar scene are acquired for improving robustness of image processing structure. On the other hand, analyze and observations a sequence of images individually are not proficient and suitable. Moreover, image fusion is an efficient approach for solving the issues through integrating corresponding information extracted out of numerous images for producing a fused solitary image[7], highly beneficial for the machine perception as well as human perception, ghost effect was resolved by Shaikh *et al*.[8] Weighted averaging involving image fusion scheme along with Tsallis entropy was investigated via researchers.[9]

Picture combination is a technique for incorporating different picture qualities into a single picture and in clinical imaging research field picture combination facilitates a fit and exact analytic methodology. Final joined pictures gained out of imaging instruments/ modalities are essential element in different areas of application, namely computer vision, geographical

*Author for Correspondence
E-mail: cs.vineeta.singh@gmail.com

imaging, microscopic imaging, medical imaging, robotics, remote sensing and so on.[10–12] Image fusion tool generated images, which are more visibly and easily identified through integrating information of numerous images of similar object. The cameras cannot replicate the panoramic outlook as source images are restricted by camera's focal length. Thus, fused images are most commonly utilized in visual perception and machine learning, while compared with other single source image. The major intention of image fusion is decreasing quantity of data during network transmission and producing new images are more precise and informative for computer processing and visual perception.[13]

The selection of clear image pixels from source regions is the fundamental idea for executing image fusion. In addition, average observed images based on particular sharpens is used for formulating fused image. Along with this, optical out of focus is a main resource of degradation of image quality in multi focus image fusion. The image fusion scheme enhances the reliability and data storage of image content and it also provides good interpretation. The following needs must be satisfied in image fusion that is image fusion process must preserve all significant information of source images, image fusion process must acquiesce several fake information. Furthermore, image fusion procedure must proficient of reducing limitations, like mis-registration.[3]

In recent years, various efficient image fusion techniques are developed using multi scale decomposition. Mainly, there are three levels at which a multi-focus image fusion strategy can be executed. First one is at pixel level, second one is decision level and last one is feature level.[14,15] Further, the multi-focus image fusion strategy is sub-categorized in two parts at pixel level i.e. transform domain as well spatial domain schemes. The approaches using spatial domain involves guided filtering[16], Principal Component Analysis[17] and image fusion techniques used human perceptions and same features[14,18] and others. In addition, fusion techniques using transform domain, which are principally analyzed in Multi resolution Geometric Analysis (MGA). Another classification of image fusion strategy involves a separation consisting of local energy functions like image fusion strategies relied on trained dictionaries, wavelets, shearlet, contourlet, discrete cosine transform as well as ripplet , artificial neural network abbreviated as ANN. For instance, shearlet along with pulse coupled neural network abbreviated as PCNN, contourlet along with PCNN, contourlet along with SCM.[15]

This research is focused to design the multi-focus image fusion through proposing Taylor ASSCA based on two input images. The contourlet transform is initially employed to input images for generation of four sub-bands for both the input images, and then the fusion technique is implemented by integrating sub-bands of image-1 and image-2 based on holoentropy and the proposed Taylor ASSCA to get the four sub-bands. Here, the Taylor-ASSCA is newly developed by incorporating Taylor series along with ASSCA where the ASSCA is the combination of ASO as well as SCA. Generated results from the fusion phase are then forwarded to the inverse contourlet transform to get the fused output image.

Major involvement of this research involves:

Developed Taylor ASSCA For Image Fusion:

An effective image fusion mechanism is developed using the proposed Taylor ASSCA for obtaining the last fused image from input image-1, and image-2. The Taylor ASSCA is the combination of Taylor series with ASSCA. Moreover, the holoentropy is also introduced with the Taylor ASSCA for choosing the optimal fusion coefficient. However, the solution with maximal MI, PSNR, UQI, SSIM, and minimal RMSE is chosen as the optimal solution using maximization fitness objective.

Related Work

Here, several present image fusion techniques with their limitations are described, which stimulate researchers for devising a new approach to execute image fusion.

Venkatrao *et al.*[12] devised a fusion strategy relied on holoentropy whale fusion i.e. HWFusion for fusing medical images. Initially for input images consideration two magnetic resonance imaging i.e. MRI images were incorporated as well as further wavelet transform was imposed to yield four sub-bands for both of the input images. Further fusion of wavelet coefficients was accompanied by utilizing two attributes i.e. whale fusion factor as well as entropy which were further assessed via holoentropy as well as SP-whale optimizer. Optimum fusion factor was selected with the help of SP-whale algorithm. At final step inverse of wavelet transform was incorporated for generation of fused image. But the devised model was unsuccessful to incorporate Bayesian model to enhance performance.[12]

Zhao *et al.*[19] devised a image fusion strategy to fuse multi-focus images utilizing deep convolutional network i.e. DCNN. For achievement of greater efficiency the resulted outputs were simultaneously under supervision during training process. But, the devised fusion model was unsuccessful for increasing performance for fusion of multi-focus images as well as convolutional neural network.

Yang *et al.*[20] devised a fusion model known as fast discrete curvelet transform i.e. FDCT to fuse multi-focus images. This model targeted two problems i.e. spatial based fusion as well as texture selection. At first, a model FDCT was developed based on frequency model involving human visual system features further developing SML technique with PCNN for extraction of frequency related comprehensive information. But the developed fusion model was unsuccessful to incorporate color images.

Huang *et al.*[21] developed an algebraic multi-grid i.e. AMG based fusion model. In this model initially grids were extracted from the source images via affinity matrix with the help of coarse grids. For approximation, there was preservation of edges as well as textual information. The calculation of MSE values were done to detect higher fidelity blocks with the help of input images. But the devised fusion technique was unsuccessful to incorporate various other metrics to assess the performance.

Li *et al.*[22] developed Deep Regression Pair Learning abbreviated as DRPL, for fusing multi-focus images. This approach was utilized for converting entire image into binary mask devoid of using patch function, and then blur point was computed in the region of defocused or focused boundary. After that, the complementary source images were taken as input for generating two binary masks for improving the performance of the system. However, the alignment between multi-focus images is the difficult task because of the presence of the camera as well as object motion.

Wen *et al.*[23] developed Convolutional Neural network abbreviated as CNN, for fusing multi-focus images. Initially, CNN was trained with clear image patches and its blurred versions for getting binary classifier. Consequently, the source images were partitioned into several overlapping patches, and then the confidence score was computed for every patch. After that, the initial clarity map was created, and refined the clarity map during consistency of verification stage to get the fused image. Here, the Mutual Information (MI) was found better, but the method needs large iteration to get the final output.

Xu *et al.*[24] designed unsupervised model using gradients as well as connected regions, termed GCF for a multi-focus image fusion. In addition, Mask-Net was introduced for generating the binary mask. Then, the gradient relation map was employed for obtaining the solution domain and accelerates the convergence. The major drawback of this method is that some mis-classified pixels, blurs or lines were still exists in the image.

Zhang *et al.*[15] devised a multi-focus image fusion strategy relied on convolutional neural network, termed as IFCNN. At first, extraction of image salient aspects was accompanied out of input images via two convolutional layers. After that, the convolutional features were fused using suitable fusion rule that was chosen based on the input image type. At last, the fused features were reconstructed for producing informative fusion image. The method failed to devise an architecture based on definite characteristics of target image database.

Most of the times multi-focus images possess de-focused/out of focused areas because of the limited availability of focused images. As a result quality level of fusion deteriorates. Zhao *et al.*[19] devised a new technique for fusing multi-focus images relied on deep convolutional neural network i.e. DCNN along with a naturally enhanced technique.

Challenges

Reinforcement to carry out proposed work via facing below challenges:

Li et al.[22] developed DRPL for fusing the multi-focus images. However, the patch-processing problem was solved effectively, but failed to use adaptive concept in the method for biomedical image fusion.

Zhang et al.[15] utilized IFCNN for fusing multi focus images. Here, the scheme is trained in end-to-end behaviour with some post-processing procedure, but still suffer from blurring or low-contrast effect.

Xu et al.[24] introduced GCF for solving stumbling block of the vanishing gradients, but the method takes more period and attempt for establishing ground truth table manually.

Zhao et al.[19] employed deep CNN for a multi-focus image fusion with enhancement. Here, performance of system was found better, but still the training of images need for fusion is very challenging.

Huang et al.[21] utilized AMG for tacking issues of multi focus image fusion in the image quality deterioration, like fake edges, ringing effects, and the

contrast decrease. However, this method does not integrate multiple metrics for eliminating the interference of the abnormal evaluation behavior.

Multi-Focus Image Fusion Using the Proposed Holoentropy and Taylor-Assisted Optimization Algorithm

This section presents the proposed Taylor ASSCA technique to combine images which are multi-focus. At first, two source images are considered as input and contourlet transform[25] is incorporated to both of the input images to generate four frequency sub-band coefficients, named as, low–low i.e. LL, high–low i.e. HL, and high–high i.e. HH as well as low–high i.e. LH. Generated four sub-bands of both the input images undergo through fusion process relied on holoentropy[26] as well as proposed Taylor–ASSCA. The development of Taylor–ASSCA is accompanied via Taylor series integration[27], ASO[28], and SCA.[29] In addition, the holoentropy identifies the fusion factor for every sub-band images using entropy computed for input image. The result obtained from the fusion phase is fed to inverse contourlet transform to get final fused image.

Generation of Four Sub Bands Using Contourlet Transform

Let us assume two input images $G(p,q)$ and $D(g,h)$ are the two input images, and it is given to CT in order to extract image sub-bands. Contourlet transform is the multiscale and the multidirectional transform in order to capture geometrical features of the 2D images. Thus, CT is more advantageous for images based on the contour as well as fine textures. Here, each band refers to the energy and frequency of the contourlet coefficient. Thus, the method is utilized to convert the functions into different frequencies, and down sampling is performed with Low pass Filter i.e. LPF as well as High pass filter i.e. HPF. Obtained contourlet bands via the application of CT have different properties. However, the down sampling and vertical filtering is devised to produce four sub-images. The low frequency images are determined by LPF by performing the convolution operation of filter and input function, and is expressed by,

$$G_L(m,n) = \sum_{u=-Rv}^{R} \sum_{=-R}^{R} [G(m,n) * L(m-u,n-v)] \quad \ldots(1)$$

$$D_L(m,n) = \sum_{u=-Rv}^{R} \sum_{=-R}^{R} [D(m,n) * L(m-u,n-v)] \quad \ldots(2)$$

The LPF function in above equations is denoted as $(m-u,n-v)$ and R represents total pixels, the symbol $*$ refer to convolution operator, and the terms $G(m,n)$ and $D(g,h)$ are the two input images. In addition, the high frequency sub images are identified using the below expression,

$$G_H(m,n) = \sum_{u=-Rv}^{R} \sum_{=-R}^{R} [G(m,n) * H(m-u,n-v)] \quad \ldots(3)$$

$$D_L(m,n) = \sum_{u=-Rv}^{R} \sum_{=-R}^{R} [D(m,n) * H(m-u,n-v)] \quad \ldots(4)$$

where, the function of HPF is denoted as $H(m-u,\ n-v$. Thus, for image Gm,n four sub band images, like $G_{LL}(m,n), G_{LH}(m,n), G_{HL}(m,n),\ G_{HH}(m,n)$ are produced. Therefore, the LL, LH, HH, HL equations of input image-1 is given by,

$$G_{LL}(m,n) = \sum_{u=-Rv}^{R} \sum_{=-R}^{R} [G_L(m,n) * L(m-u,n-v)] \quad \ldots(5)$$

$$G_{LH}(m,n) = \sum_{u=-Rv}^{R} \sum_{=-R}^{R} [G_L(m,n) * H(m-u,n-v)] \quad \ldots(6)$$

$$G_{HL}(m,n) = \sum_{u=-Rv}^{R} \sum_{=-R}^{R} [G_H(m,n) * L(m-u,n-v)] \quad \ldots(7)$$

$$G_{HH}(m,n) = \sum_{u=-Rv}^{R} \sum_{=-R}^{R} [G_H(m,n) * H(m-u,n-v)] \quad \ldots(8)$$

where, the low frequency coefficient matrix is denoted as $G_L(m,n)$ as well as the term as $G_H(m,n)$, refer to high frequency coefficient matrix.

For $D(m,n)$, four contourlet coefficient matrices, such as $D_{LL}(m,n), D_{LH}(m,n),\ D_{HL}(m,n), D_{HH}(m,n)$ are produced.

Image Fusion Using Holoentropy and the Proposed Taylor ASSCA

Once the transformation of source images is accomplished to yield four frequency sub-band coefficients, the process of image fusion is incorporated utilizing holoentropy as well as the developed Taylor ASSCA. The Taylor ASSCA is developed newly by combining Taylor series along with atom search sine cosine algorithm abbreviated as ASSCA. The holoentropy and the proposed Taylor ASSCA is briefly explained below.

Holoentropy-Based Image Fusion

This sub–section explains holoentropy approach for fusing multi-focus images through calculating joint

fusion probability in every image sub bands. Entropy becomes popular metric, which is utilized for fusing the image. If fused image possess higher amount of information extracted out of the source image; value gained via entropy is low; hence the better result cannot be obtained. Therefore, holoentropy has been introduced for measuring the unpredictability of the information present in the image. The better feature search is achievable in holoentropy than entropy-based procedure. The proposed fusion rule is defined by weighted coefficient by considering every sub band is expressed by,

$$P = \alpha G + (1-\alpha) D \quad \ldots(9)$$

where, $\alpha = \frac{\alpha^T + \alpha^{\hbar}}{2}$. Here, α^T refer to fusion factor based on the proposed Taylor ASSCA, $\alpha^{\hbar}$ signifies the fusion factor using holoentropy. The fusion principle relied on the weighted coefficient for fusing image sub bands may be illustrated as,

$$P_{LL}(m,n) = \alpha G_{LL}(m,n) - (1-\alpha) D_{LL}(m,n) \quad \ldots(10)$$

$$P_{LH}(m,n) = \alpha G_{LH}(m,n) - (1-\alpha) D_{LH}(m,n) \quad \ldots(11)$$

$$P_{HL}(m,n) = \alpha G_{HL}(m,n) - (1-\alpha) D_{HL}(m,n) \quad \ldots(12)$$

$$P_{HH}(m,n) = \alpha G_{HH}(m,n) - (1-\alpha) D_{HH}(m,n) \quad \ldots(13)$$

The fused sub image coefficients are computed using holoentropy and Taylor ASSCA in which the Taylor ASSCA is elaborated in below section.

Optimal Fusion Coefficient Selection using the Developed Taylor ASSCA

The developed Taylor ASSCA is utilized in order to select the best optimal fusion coefficient for better image fusion. The Taylor ASSCA is a new fusion approach by incorporating Taylor series and ASSCA. Complex variables are described through Taylor series, which is expansion of the function into limitless summation of terms. It helps for assessing integrals as well as infinite summations via recognizing Taylor series. In addition, dealing of higher order terms in a single step through Taylor series is an effective way. In addition, the system can easily resolve non-linear issues with the difficult restrictions. On the other hand, ASSCA provides the better trade-off among the exploitation and exploration, which includes efficiency to developed method. Additionally, the method boosts up the convergence process and improved the solution diversity and performance. Thus, the combination of Taylor series and ASSCA is carried out for improving the overall system performance of algorithm.

Solution Encoding

Solution encoding is a illustration of solution vector in order to select the optimal fusion factor that is produced the fusion probability for fusing sub-image coefficients. Let us assume $Z_r = \{Z_1, Z_2, \ldots, Z_x\}$ be the solution set containing x quantity of solutions. Here, every solution in Z_r is the group with dimension $1 \times n$, where n refer to number of the produced parameters. From the solution x, the proposed Taylor ASSCA selects the optimal solution using the fitness function to compute the best fusion coefficient value.

Steps followed in developed Taylor ASSCA are demonstrated as.

Step 1: Initialization

The solution is initialized in first step in the random way along with another algorithmic parameters expressed by,

$$J = \{J_1, J_2, \cdots, J_c, \cdots, J_m\}; 1 < c \le m \quad \ldots(14)$$

where, the term J_c refer to c^{th} solution, and the total solutions is indicated as m.

Step 2: Computation of fitness

The objective function is estimated using fitness function equation for every solution. However, fitness function is considered as maximization function where the solution with minimum fitness value is chosen as best solution. However, function used to compute the fitness is expressed by,

$$E = \frac{1}{2}\left[E_1 + E_2\right] \quad \ldots(15)$$

where, the term E_1 signifies the fitness function based on variables, and the mathematical model is given by,

$$E_1 = \frac{1}{5}\left[E_M + E_{\mathrm{P}} + E_L + E_S + E_U\right] \quad \ldots(16)$$

where, the term E_M, E_{P}, E_L, E_S, and E_U represents the function mutual information, PSNR, RMSE,

SSIM, and UQI. The fitness function using Joint Holoentropy is denoted as E_2, and is expressed by,

$$E_2 = X(G, D, V) \quad \ldots(17)$$

where, the terms G, and D represents the two input images and V fused image.

Step 3: Update solution based on developed Taylor ASSCA

The update process of developed Taylor ASSCA is done through combining Taylor series with ASSCA. The update equation of ASSCA is expressed by Eq. 18 where, $J_c(y)$ depicts position of c^{th} atom at y iteration and $J_c(y+1)$ utilized to denote the update position of c^{th} atom at iteration *(y+1)* and, A_{BEST} shows best fitness value, M depicts highest number of iterations, $Rand_c, Rand_f$ depicts random numbers generated in [0,1], $a_c(y)$ depicts velocity of c^{th}atom at y iteration, β denotes depth weight, $P_a(b)$ depicts mass of a^{th} atom at b^{th} iteration. η depicts multiplier weight. || depicts absolute value.

Let

$$Y = \beta\left(1-\frac{y-1}{M}\right)^3 e^{\frac{-20y}{M}} \sum_{f\in A_{BEST}} \frac{Rand_f\left[2\times\left(l_{cf}(y)\right)^{13} - l_{cf}^7\right]}{p_a(b)} \frac{J_f(y)-J_c(y)}{\| J_f(y), J_c(y)\|_2}$$

where A_{BEST} shows best fitness value, M depicts highest number of iterations, $Rand_c$, depicts random number in [0,1], β denotes depth weight, Here $P_a(b)$ depicts mass while η depicts multiplier weight. || depicts absolute value. Then, Eq. 18 is rearranged as Eq. 19.

To enhance performance of the system and to solve optimization problems of ASSCA, Taylor series is utilized. As per Taylor series, the update equation is given by, Eq. 20, further Eq. 20 may be rearranged as Eq. 21.

Thereafter, substituting Eq. 21 in Eq. 19, the solution is depicted through Eq. 22, where, velocity is denoted as $a_c(y)$, the depth weight is indicated as β, the term η refer to multiplier weight, and the mass is represented as $p_a(b)$, g_1 depicts direction of movement, g_2 depicts how far the movement has to be whether in opposite direction or in same direction of the target, g_3 facilitates arbitrary weight to target. After arranging terms of Eq. 22, it can be represented as Eq. 23.

$$J_c(y+1) = \frac{g_1 g_3 Sin(g_2) d_c(y)}{g_1 g_3 Sin(g_2) d_c(y) - \eta e^{\frac{-20y}{M}}} \left[\begin{array}{l} J_c(y) + Rand_c a_c(y) - \beta\left(1-\frac{y-1}{M}\right)^3 e^{\frac{-20y}{M}} \sum_{f\in A_{BEST}} \frac{Rand_f\left[2\times\left(l_{cf}(y)\right)^{13} - l_{cf}^7\right]}{p_a(b)} \\ \frac{J_f(y)-J_c(y)}{\| J_f(y), J_c(y)\|_2} - \frac{\eta e^{\frac{-20y}{M}} J_c(y)\left[1 - g_1 Sin(g_2) + g_1 g_3 Sin(g_2)\right]}{g_1 g_3 Sin(g_2) d_c(y)} \end{array} \right] \quad \ldots(18)$$

$$J_c(y+1) = \frac{g_1 g_3 Sin(g_2) d_c(y)}{g_1 g_3 Sin(g_2) d_c(y) - \eta e^{\frac{-20y}{M}}} \left[J_c(y) + Rand_c a_c(y) - Y - \frac{\eta e^{\frac{-20y}{M}} J_c(y)\left[1 - g_1 Sin(g_2) + g_1 g_3 Sin(g_2)\right]}{g_1 g_3 Sin(g_2) d_c(y)} \right] \quad \ldots(19)$$

$$\begin{array}{l} J_c(y+1) = 0.5 J_c(y) + 1.3591 J_c(y-1) - 1.359 J_c(y-2) + 0.6795 J_c(y-3) \\ - 0.2259 J_c(y-4) + 0.0555 J_c(y-5) - 0.0104 J_c(y-6) + 1.38 e^{-3} J_c(y-7) - 9.92 e^{-5} J_c(y-8) \end{array} \quad \ldots(20)$$

$$J_c(y) = 2\left[\begin{array}{l} J_c(y+1) - 1.3591 J_c(y-1) + 1.359 J_c(y-2) - 0.6795 J_c(y-3) \\ + 0.2259 J_c(y-4) - 0.0555 J_c(y-5) D + 0.0104 J_c(y-6) - 1.38 e^{-3} J_c(y-7) + 9.92 e^{-5} J_c(y-8) \end{array} \right] \quad \ldots(21)$$

$$J_c(y+1) = \frac{g_1 g_3 Sin(g_2) d_c(y)}{g_1 g_3 Sin(g_2) d_c(y) - \eta e^{\frac{-20y}{M}}} \left[J_c(y)\left(1 - \eta e^{\frac{-20y}{M}} \frac{\left[1 - g_1 Sin(g_2) + g_1 g_3 Sin(g_2)\right]}{g_1 g_3 Sin(g_2) d_c(y)}\right) + Rand_c a_c(y) - Y \right] \quad \ldots(22)$$

$$\begin{array}{l} J_c(y+1)\left[1 - \frac{2 g_1 g_3 Sin(g_2) d_c(y)}{g_1 g_3 Sin(g_2) d_c(y) - \eta e^{\frac{-20y}{M}}}\right]\left(1 - \eta e^{\frac{-20y}{M}}\left(\frac{1 - g_1 Sin(g_2) + g_1 g_3 Sin(g_2)}{g_1 g_3 Sin(g_2) d_c(y}\right)\right) = \frac{g_1 g_3 Sin(g_2) d_c(y)}{g_1 g_3 Sin(g_2) d_c(y) - \eta e^{\frac{-20y}{M}}} \\ \left[2\left[\begin{array}{l} J_c(y+1) - 1.3591 J_c(y-1) + 1.359 J_c(y-2) - 0.6795 J_c(y-3) \\ + 0.2259 J_c(y-4) - 0.0555 J_c(y-5) + 0.0104 J_c(y-6) - 1.38 e^{-3} J_c(y-7) + 9.92 e^{-5} J_c(y-8) \end{array} \right]\left(1 - \eta e^{\frac{-20y}{M}}\left(\frac{1 - g_1 Sin(g_2) + g_1 g_3 Sin(g_2)}{g_1 g_3 Sin(g_2) d_c(y}\right)\right)\right] - Y + Rand_c a_c(y) \end{array} \quad \ldots(23)$$

The final update equation of the proposed Taylor ASSCA for better image fusion is expressed through Eq. 24 where,

$$Y=\beta\left(1-\frac{y-1}{M}\right)^{3} e^{\frac{-20y}{M}} \sum_{f\in A_{BEST}} \frac{Rand_f\left[2\times\left(l_{cf}(y)\right)^{13}-l_{cf}^{7}\right]}{p_a(b)} \frac{J_f(y)-J_c(y)}{\|J_f(y),J_c(y)\|_2}$$

and the velocity is denoted as $a_c(y)$, the depth weight is indicated as β, the term η refer to multiplier weight, and the mass is represented as $p_a(b)$. g_1 depicts direction of movement, g_2 depicts how far the movement has to be whether in opposite direction or in same direction of the target.

Step 4: Re-evaluate fitness:

The fitness value is estimated by the objective function specified in Eq. 15 such that the fitness measure with minimal value is declared as best solution.

Step 5: Termination:

Until the best solution is attained for multi-focus image fusion, the aforementioned steps are repeated.

Results and Discussion

In this section comparative analysis of developed strategy with the existing strategies has been illustrated through key performance indicators.

Experimental Details

The implementation of developed approach has been done through MATLAB via PC along with the Intel i3 core processor, Windows 10 operating system and 2GB RAM. The experimentation has been performed on Lytro Multi-focus Image Dataset.[30] This database involves 20 color multi-focus image pairs. Each image size is of 520×520 pixels. This image dataset is available publically online. In addition, four triplets of the multi-focus images i.e. three source images of a single scene and total of four such series, are also the part of dataset. The performance values have been demonstrated through Tables 1 and 2 for MI, UQI, PSNR, SSIM, RMSE metrics. Graphical representation of the analysis has been demonstrated through Figs 1–3.

Performance Evaluation Metrics

The performance of developed Contourlet + Taylor ASSCA is performed to analyze various techniques with respect to metrics, Root Mean Square Error abbreviated as RMSE, universal quality index, in short UQI, Peak Signal to Noise Ratio, in short PSNR, and structural similarity index measure i.e. SSIM as well as mutual information i.e. MI.

a) RMSE:

It is defined to compute the fusion model error for predicting the quantitative data, and is given by,

$$L=\frac{1}{2}[L[G(m,n),V(m,n)]+L[D(m,n),V(m,n)]] \quad \ldots (25)$$

where, the two input images are indicated as $G(m,n)$, $D(m,n)$, and the fused image is represented as $V(m,n)$. Minimum value of RMSE denotes the better performance in context of a good image fusion technique.

b) UQI:

It is the metric that measures first and second order statistic of two images, and is expressed as,

$$U=\frac{4\mu_G\mu_D\mu_{G,D}}{(\mu_G^2+\mu_D^2)(\sigma_G^2+\sigma_D^2)} \quad \ldots (26)$$

where, μ_G and μ_D indicate the mean value of two images, while σ_G as well as σ_D are the variance of two images. UQI value closer to +1 denotes effective algorithm.

c) *PSNR:*

The definition for peak signal to noise ratio may be given as ratio between highest attainable signal power and power of affected noise where highest value for peak signal to noise ratio points towards better performing result and decibel (dB) is used to denote PSNR.

$$PSNR=10\log_{10}\left(\frac{m_{\max}^{\ 2}}{MSE}\right) \quad \ldots (27)$$

In Eq. 27 $m_{\max}$ has been used for indicating maximum image pixel value while mean square error has been represented through MSE

$$J_c(y+1)=\left[1-\frac{2g_1g_3Sin(g_2)d_c(y)}{g_1g_3Sin(g_2)d_c(y)-\eta e^{\frac{-20y}{M}}}\left(1-\eta e^{\frac{-20y}{M}}\left(\frac{1-g_1Sin(g_2)+g_1g_3Sin(g_2)}{g_1g_3Sin(g_2)d_c(y}\right)\right)\right]^{-1}\frac{g_1g_3Sin(g_2)d_c(y)}{g_1g_3Sin(g_2)d_c(y)-\eta e^{\frac{-20y}{M}}}$$
$$\left[2\begin{bmatrix}1.359J_c(y-2)-1.3591J_c(y-1)-0.6795J_c(y-3)\\+0.2259J_c(y-4)-0.0555J_c(y-5)+0.0104J_c(y-6)-1.38e^{-3}J_c(y-7)+9.92e^{-5}J_c(y-8)\end{bmatrix}-Y+Rand_c a_c(y)\right] \quad \ldots(24)$$

Table 1 — Performance Analysis using db2, coif1, sym2 for fusion quality metrics RMSE, UQI, PSNR, SSIM, MI for image pair 1 (Bold font: best performance results)

S. No.	Three Transforms	Metrics	DWT+ UDWT +GA	DWT+ DCNN	DWT+ HWFusion +SP-Whale	DWT+ ASSCA+ Renyi entropy	Proposed Method
1	db2	RMSE	8.826	7.650	8.827	7.650	**3.687**
2		UQI	0.968	0.968	0.965	0.969	0.974
3		PSNR(dB)	33.38	30.45	33.39	35.69	38.81
4		SSIM	0.901	0.890	0.886	0.898	0.902
5		MI	1.330	1.258	1.331	1.393	1.562
1	coif1	RMSE	8.826	7.650	8.728	7.650	5.598
2		UQI	0.973	0.971	0.973	0.976	0.979
3		PSNR(dB)	33.38	31.91	33.05	40.62	**42.08**
4		SSIM	0.886	0.914	0.920	0.923	0.929
5		MI	1.334	1.294	1.322	1.492	**1.651**
1	sym2	RMSE	8.827	7.650	9.142	7.650	6.276
2		UQI	0.973	0.976	0.973	0.981	**0.984**
3		PSNR(dB)	33.39	33.35	34.82	35.69	37.77
4		SSIM	0.890	0.913	0.902	0.926	**0.943**
5		MI	1.331	1.331	1.364	1.393	1.589

Table 2 — Performance Analysis using db2, coif1, sym2 for fusion quality metrics RMSE, UQI, PSNR, SSIM, MI for image pair 5 (Italic font: better performance results)

S. No.	Three transforms	Metrics	DWT+ UDWT +GA	DWT +DCNN	DWT+ HWFusion +SP-Whale	DWT+ ASSCA +Renyi entropy	Proposed Method
1	db2	RMSE	43.97	43.75	44.02	43.75	*42.53*
2		UQI	0.96	0.960	0.963	0.965	*0.966*
3		PSNR(dB)	18.67	19.79	20.10	23.08	*25.95*
4		SSIM	0.841	0.874	0.848	0.880	*0.888*
5		MI	1.143	1.156	1.169	1.235	*1.389*
1	coif1	RMSE	44.02	43.75	43.94	43.75	*40.25*
2		UQI	0.967	0.963	0.964	0.971	*0.973*
3		PSNR(dB)	19.79	19.79	18.20	23.20	*26.81*
4		SSIM	0.869	0.845	0.857	0.889	*0.896*
5		MI	1.162	1.156	1.134	1.230	*1.372*
1	*Sym2*	RMSE	44.06	43.75	44.02	43.75	*40.79*
2		UQI	0.962	0.960	0.996	0.974	*0.979*
3		PSNR(dB)	20.35	19.79	19.78	20.66	*22.95*
4		SSIM	0.845	0.841	0.846	0.856	*0.913*
5		MI	1.174	1.156	1.162	1.180	*1.356*

d) ***SSIM Index:***

We may utilize this SSIM index as a key performing indicator for comparing two images. Highest value for SSIM index points towards better performing result.

$$SSIM(\mathrm{K},\mathrm{H}) = \frac{(2\eta_{\mathrm{K}}\eta_{\mathrm{H}} + \varphi_1)(2\xi_{\mathrm{KH}} + \varphi_2)}{(\eta_{\mathrm{K}}{}^2 + \eta_{\mathrm{H}}{}^2 + \varphi_1)(\xi_{\mathrm{K}}{}^2 + \xi_{\mathrm{H}}{}^2 + \varphi_2)} \quad \ldots (28)$$

where, K, and H are notations used to depict pixels moreover η_{K} and η_{H} used to denote mean pixel value, ξ_{K} and ξ_{H} used to denote variance of pixels and ξ_{KH} denotes the covariance of pixels, further φ_1 and φ_2 used to denote variables utilized for stabilization.

e) MI:

It is utilized to measure the quantity of the mutual dependence between the two images, moreover MI value is computed using the below expression.

$$M = \frac{1}{2}[M[G(m,n),V(m,n)]M[D(m,n),V(m,n)]] \quad \ldots(29)$$

where, the two input images are indicated as $\mathrm{G}(\mathrm{m},\mathrm{n})$, $\mathrm{D}(\mathrm{m},\mathrm{n})$, and the fused image is represented

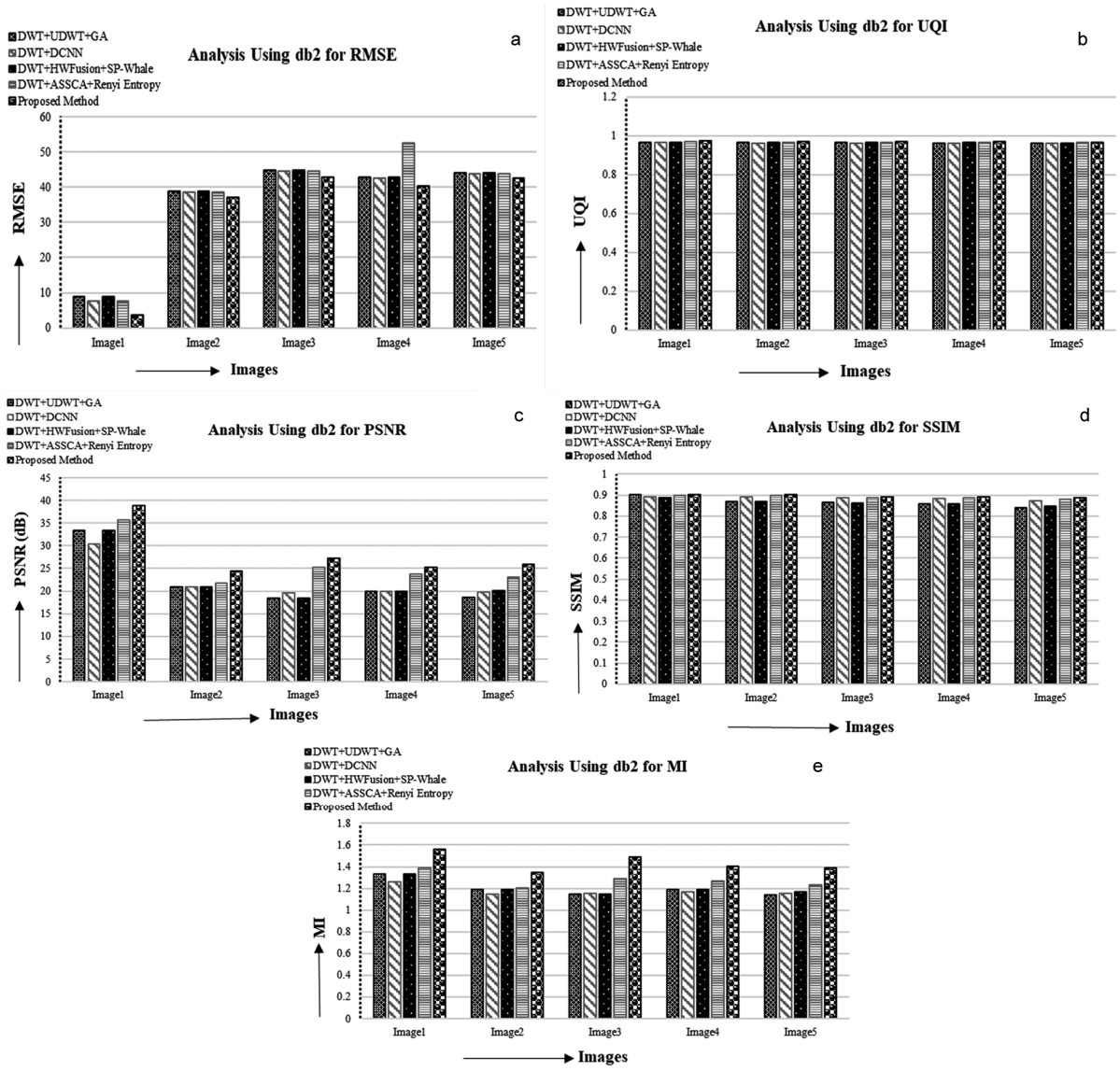

Fig. 1 — Analysis of methods based on db2 contourlet transform a) RMSE b) UQI, c) PSNR, d) SSIM, and e)MI

as $V(m, n)$. Higher value of the MI denotes better performance.

Experimental Results and Comparative Techniques

The experimentation is performed on Lytro Multi-focus Image Dataset for performing multi focus image fusion. The methods, like DWT + DCNN[19], DWT + HWFusion + SP-Whale[12], DWT + ASSCA + Renyi entropy[31] as well as DWT + UDWT + GA[32] are utilized for comparison with proposed Contourlet +Taylor ASSCA for the analysis. Parameter constants for proposed fusion model involved number of iterations = 10. The analysis is carried out based on Daubechies 2 (db2), coiflets 1 (Coif1), and symlets 2 (Sym2).

a) Analysis of Image Fusion With Respect to db2

The comparative analysis in terms of metrics for image fusion relied on db2 is portrayed in Fig 1. Analysis using RMSE metric, UQI metric, PSNR metric, SSIM metric and MI metric respectively with different images are shown in Fig 1a), Fig 1b), Fig 1c), Fig 1d), Fig 1e).

b) Analysis of Image Fusion In Terms of Coif1

The analysis of methods in terms of metrics for image fusion based on Coif1 is depicted in Fig. 2 where Fig 2a), Fig 2b), Fig 2c), Fig 2d), Fig 2e) illustrates analysis using, RMSE metric, UQI metric, PSNR metric, SSIM metric, MI metric respectively with different images.

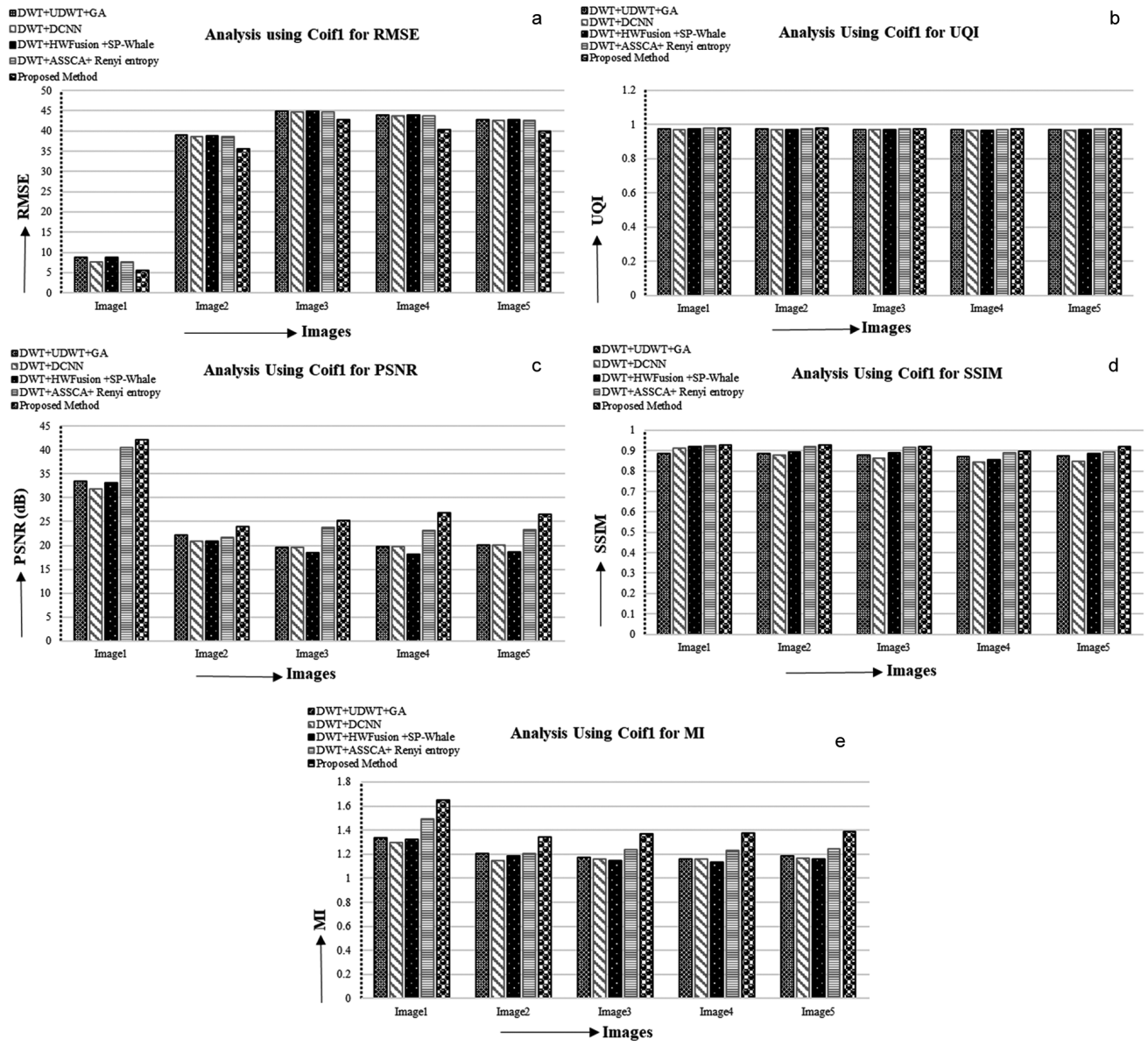

Fig. 2 — Analysis of methods based on Coif1 contourlet transform a) RMSE b)UQI , c)PSNR, d) SSIM, and e)MI

c) Analysis of The Image Fusion Based on Sym2

The comparative analysis based on sym2 for image fusion is displayed in Fig. 3 where Fig. 3a), Fig. 3b), Fig. 3c), Fig. 3d), Fig. 3e) portrays the analysis using RMSE metric, UQI metric, PSNR metric, , SSIM metric, MI metric with different images respectively.

Comparative Discussion

We have demonstrated different performance metrics (MI, PSNR, RMSE, UQI, SSIM) through Table 1, Table 2 as well as via Fig. 1, Fig. 2, Fig. 3 comparative analysis comparison with existing algorithms to proposed method using db2, coif1 and sym2 respectively. The maximal MI yielded through the developed Contourlet + Taylor ASSCA with the value of **1.651**, using coif1. The maximal PSNR computed by proposed Contourlet + Taylor ASSCA with a value of **42.08dB** based on coif1. In addition, the maximal UQI computed by proposed Contourlet + Taylor ASSCA with a value of **0.984**, based on sym2. The minimal RMSE computed by proposed Contourlet + Taylor ASSCA with a value of **3.687**, based on db2. The maximal SSIM computed by proposed Contourlet + Taylor ASSCA with a value of **0.943** based on sym2.

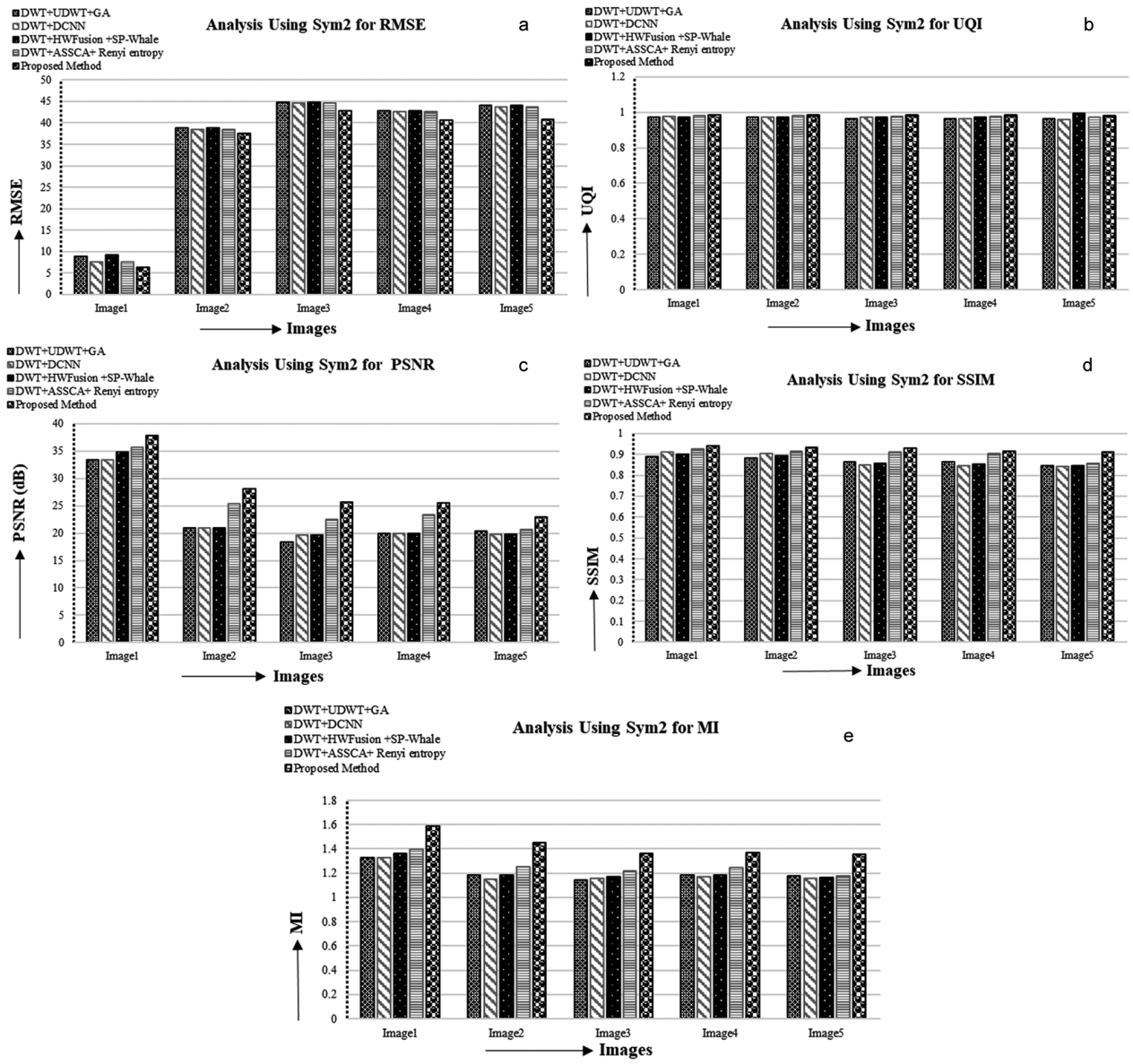

Fig. 3 — Analysis of methods based on sym2 contourlet transform a) RMSE b) UQI, c) PSNR, d) SSIM, e) MI

Conclusions and Future Scope

This paper incorporates the proposed HoEnTOA to combine/fuse multi-focus images. Moreover, contourlet transform is introduced for converting two input images further generating four frequency sub-band coefficients, such as LH, LL, HH as well as HL. Once the sub-band is made, proposed Taylor ASSCA and the holoentropy are employed for fusing weighted function in order to fuse the images. Here, the Taylor ASSCA is designed newly by incorporating ASSCA with Taylor series. Once the fusion is done, the inverse contourlet transform is executed to gain final fused image. Here, the fusion is done with respect to maximal fitness function. Thus, proposed HoEnTOA performs the image fusion effectively. The experimentation is carried out based on Lytro Multi-focus color image dataset. The devised image fusion scheme has demonstrated the better performance via the metrics MI, PSNR, RMSE, UQI, and SSIM. The effectiveness of proposed model is computed which revealed *maximal MI* of **1.651**, *maximal PSNR* of **42.08 dB**, *maximal UQI* of **0.984**, *maximal SSIM* of **0.943**, and *minimal RMSE* of **3.687**, respectively. In future, Bayesian theory may be further incorporated to the proposed model.

References

1 Panigrahy C, Seal A, Mahato N K, Krejcar O & Herrera-Viedma E, Multi-focus image fusion using fractal dimension, *Appl Opt*, **59** (2020) 5642–*5655*.

2 Xiao B, Ou G, Tang H, Bi X & Li W, Multi-focus image fusion by hessian matrix based decomposition, *IEEE Trans Multimedia*, **22(2)** (2019) 285–*2*97.

3 Amin-Naji M & Aghagolzadeh A, Multi-focus image fusion in DCT domain using variance and energy of Laplacian and correlation coefficient for visual sensor networks, *J Artif Intell Data Min*, **6(2)** (2018) 233–250.

4 Guo X, Nie R, Cao J, Zhou D, Mei L & He K, FuseGAN: Learning to fuse multi-focus image via conditional generative adversarial network, *IEEE Trans Multimedia*, **21(8)** (2019) 1982–1996.

5 Liu Y, Wang L, Cheng J, Li C & Chen X, Multi-focus image fusion: A survey of the state of the art, *Inf Fusion*, **64** (2020) 71–91.

6 Ma J, Liang P, Yu W, Chen C, Guo X, Wu J & Jiang J, Infrared and visible image fusion via detail preserving adversarial learning, *Inf Fusion*, **54** (2020) 85–98.

7 Kaur H, Koundal D & Kadyan V, Image fusion techniques: a survey, *Arch Comput Methods Eng*, (2021) 1–23.

8 Shaikh U A, Vishwakarma VJ & Mahale S S, Dynamic scene multi-exposure image fusion, *IETE J Educ*, **59(2)** (2018) 53–61.

9 Sholehkerdar A, Tavakoli J & Liu Z, Theoretical analysis of Tsallis entropy-based quality measure for weighted averaging image fusion, *Inf Fusion*, **58** (2020) 69–81.

10 Borsoi R A, Imbiriba T, & Bermudez J C, Super-resolution for hyperspectral and multispectral image fusion accounting for seasonal spectral variability, *IEEE Trans Image Process,* **29** (2019) 116–127.

11 Du J, Li W & Tan H, Intrinsic image decomposition-based grey and pseudo-color medical image fusion, *IEEE Access*, **7** (2019) 56443–56456.

12 Venkatrao P H & Damodar S S, HWFusion: Holoentropy and SP-Whale optimisation-based fusion model for magnetic resonance imaging multimodal image fusion, *IET Image Process*, **12(4)** (2017) 572–581.

13 Fu Y, Wu X J & Durrani T, Image fusion based on generative adversarial network consistent with perception, *Inf Fusion,* **72** (2021) 110–125.

14 Jing Z, Pan H, Li Y & Dong P, Evaluation of focus measures in multi-focus image fusion, in *Non-cooperative Target Tracking, Fusion and Control* (Springer, Cham) 2018 269–281.

15 Zhang Y, Liu Y, Sun P, Yan H, Zhao X & Zhang L, IFCNN: A general image fusion framework based on convolutional neural network, *Inf Fusion*, **54** (2020) 99–118.

16 Qiu X, Li M, Zhang L & Yuan X, Guided filter-based multi-focus image fusion through focus region detection, *Signal Process Image Commun*, **72** (2019) 35–46.

17 Yang Y, Ding M, Huang S, Que Y, Wan W, Yang M & Sun J, Multi-focus image fusion via clustering PCA based joint dictionary learning, *IEEE Access*, **5** (2017) 16985–16997.

18 Wang K, Qi G, Zhu Z & Chai Y, A novel geometric dictionary construction approach for sparse representation based image fusion, *Entropy,* **19(7)** (2017) 306.

19 Zhao W, Wang D & Lu H, Multi-focus image fusion with a natural enhancement via a joint multi-level deeply supervised convolutional neural network, *IEEE Trans Circuits Syst Video Technol*, **29(4)** (2018) 1102–1115.

20 Yang Y, Tong S, Huang S, Lin P & Fang Y, A hybrid method for multi-focus image fusion based on fast discrete curvelet transform, *IEEE access,* **5** (2017) 14898–14913.

21 Huang Y, Li W, Gao M & Liu Z, Algebraic multi-grid based multi-focus image fusion using watershed algorithm, *IEEE Access*, **6** (2018) 47082–47091.

22 Li J, Guo X, Lu G, Zhang B, Xu Y,Wu F & Zhang D, DRPL: Deep regression pair learning for multi-focus image fusion, *IEEE Trans Image Process*, **29** (2020) 4816–4831.

23 Wen Y, Yang X, Celik T, Sushkova O & Albertini M K, Multifocus image fusion using convolutional neural network, *Multimed Tools Appl*, **79(45)** (2020) 34531–34543.

24 Xu H, Fan F, Zhang H, Le Z & Huang J, A deep model for multi-focus image fusion based on gradients and connected regions, *IEEE Access*, **8** (2020) 26316–26327.

25 Hasan M M, Islam N, & Rahman M M (2020). Gastrointestinal polyp detection through a fusion of contourlet transform and Neural features, *J King Saud Univ, Comp & Info Sci*, (2020).

26 Mane V M & Jadhav D V, Holoentropy enabled-decision tree for automatic classification of diabetic retinopathy using retinal fundus images, *Biomed Tech (Berl)*, **62(3)** (2017) 321–332.

27 Mangai S A, Sankar B R & Alagarsamy K, Taylor series prediction of time series data with error propagated

28 by artificial neural network, *Int J Comput Appl*, **89(1)** (2014).

29 Zhao W, Wang L & Zhang Z, Atom search optimization and its application to solve a hydrogeologic parameter estimation problem, *Knowl Based Syst*, **163** (2019) 283–304.

30 Mirjalili S, SCA: a sine cosine algorithm for solving optimization problems, *Knowl Based Syst*, **96** (2016) 120–133.

31 Nejati M, Samavi S & Shirani S, Multi-focus image fusion using dictionary-based sparse representation, *Inf Fusion*, **25** (2015) 72–84.

32 Singh V & Kaushik V D, Renyi entropy and atom search sine cosine algorithm for multi focus image fusion, *Signal Image Video Process*, **15** (2021) 903–912.

33 Kavitha S & Thyagharajan K K, Efficient DWT-based fusion techniques using genetic algorithm for optimal parameter estimation, *Soft Comput*, **21(12)** (2017) 3307–3316.